

Article

Pathways to the Local Thermodynamic Equilibrium of Complex Autoionizing States

Frédéric Petitdemange¹ and Frank B. Rosmej^{1,2,*}

¹ Faculty of Science & Engineering, Sorbonne University, UMR 7605, Case 128, 4 Place Jussieu, F-75252 Paris, France

² Ecole Polytechnique, Laboratoire pour l'Utilisation des Lasers Intenses (LULI), Atomic Physics in Dense Plasmas, Route de Saclay, F-91229 Palaiseau, France

* Correspondence: frank.rosmej@sorbonne-universite.fr

Abstract: The generally accepted pathway to Local Thermodynamic Equilibrium (LTE) in atomic physics, where collision rates need to be much larger than radiative decay rates, is extended to complex autoionizing states. It is demonstrated that the inclusion of the non-radiative decay (autoionization rate) on the same footing, like radiative decay, i.e., the LTE criterion $n_{e,crit} \times C \gg A + \Gamma$ ($n_{e,crit}$ is the critical electron density above which LTE holds, C is the collisional rate coefficient, and A is the radiative decay rate) is inappropriate for estimating the related critical density. An analysis invoking simultaneously different atomic ionization stages identifies the LTE criteria as a theoretical limiting case, which provides orders of magnitude too high critical densities for almost all practical applications. We introduced a new criterion, where the critical densities are estimated from the non-autoionizing capture states rather than from the autoionizing states. The new criterion is more appropriate for complex autoionizing manifolds and provides order of magnitude reduced critical densities. Detailed numerical calculations are carried out for Na-like states of aluminum, where autoionization to the Ne-like ground and excited state occurrences are in excellent agreement with the new criterion. In addition, a complex multi-electron atomic-level structure and electron–electron correlation are identified as simplifying features rather than aggravating ones for the concept of thermalization.



Citation: Petitdemange, F.; Rosmej, F.B. Pathways to the Local Thermodynamic Equilibrium of Complex Autoionizing States. *Atoms* **2023**, *11*, 146. <https://doi.org/10.3390/atoms11110146>

Academic Editor: Jean-Christophe Pain

Received: 17 September 2023

Revised: 29 October 2023

Accepted: 6 November 2023

Published: 15 November 2023



Copyright: © 2023 by the authors. Licensee MDPI, Basel, Switzerland. This article is an open access article distributed under the terms and conditions of the Creative Commons Attribution (CC BY) license (<https://creativecommons.org/licenses/by/4.0/>).

Keywords: autoionization; local thermodynamic equilibrium; inner-shell excitation; atomic kinetics; absolute and relative intensities

1. Introduction

Analysis of radiative properties plays a key role in advancing high-density matter research and it is quantitative spectroscopy that has considerably progressed the field [1–8], including dense plasma effects on atomic structure and elementary processes [5,6,9–11]. The fundamental quantities are the atomic populations that have to be obtained from population kinetics, taking into account all relevant collisional-radiative processes. Traditional spectroscopy is based on the analysis of resonance line emissions [1,2] that originate from single excited states. Autoionizing states, however, are multiple-excited states from which the so-called dielectronic satellite emission originates. This emission is of particular interest for the advanced analyses (supra-thermal electrons, transient matter evolution, spatial non-homogeneity, opacity, and radiation field) of radiative properties [6].

For autoionizing states, the atomic population kinetic collisional-radiative approach becomes readily extremely complex because of the large number of atomic levels involved, even for rather simple configurations. The concept of validity criteria for local thermodynamic equilibrium (LTE) is therefore of great importance. Although well established for non-autoionizing states [1], the complexity of multiple-excited core hole atomic states does not allow for the development of simple and general criteria.

It is the purpose of the present article to analyze the possible pathways to the local thermodynamic equilibrium of autoionizing states and shed more light on LTE validity criteria and their use in estimating critical densities.

2. Criteria for Local Thermodynamic Equilibrium

The spectral distribution of local plasma emission is given by:

$$I_{\omega}^{(Z)} = \sum_i \sum_{j>i} \frac{\hbar\omega_{ji}^{(Z)}}{4\pi} \cdot n_j^{(Z)} \cdot A_{ji}^{(Z)} \cdot \varphi_{ji}^{(Z)}(\omega) \tag{1}$$

where $I_{\omega}^{(Z)}$ is the spectral distribution originating from charge state Z , i and j are the atomic levels in the various charge states $Z = 0, 1, \dots, Z_n$ (Z_n is the nuclear charge), $A_{ji}^{(Z)}$ is the spontaneous transition probability, $\omega_{ji}^{(Z)}$ is the transition angular frequency, $\varphi_{ji}^{(Z)}(\omega)$ is the line profile, and $n_j^{(Z)}$ is the atomic/ionic population density.

One of the most powerful methods for determining atomic/ionic populations is the concept of local thermodynamic equilibrium. When the LTE holds true, the atomic population density is given by:

$$n_j^{(Z)} = \frac{g_j^{(Z)}}{\Xi(Z)} \cdot \exp\left(-\frac{E_j^{(Z)}}{k_B T_e}\right) \tag{2}$$

where $g_j^{(Z)}$ is the statistical weight of level j , $\Xi(Z)$ is the partition function, $E_j^{(Z)}$ is the energy of the state j , and T_e is the electron temperature. When Equation (2) holds true, the complex task for calculating $n_j^{(Z)}$ is circumvented. The application of Equation (2) to all atomic/ionic states considerably simplifies the determination of atomic populations. In fact, Equation (2) would also concern ground states and all charge states that would then necessarily be connected by the well-known Saha-relation. The related critical density may easily exceed the solid density (in particular for highly charged ions) and is therefore of little practical interest.

More appropriate is the application of Equation (2) just to autoionizing states of certain configurations, thereby still permitting a large reduction in numerical burden while conserving the possibility of following transient plasma evolution and non-LTE population for resonance line emission [12]. If $\{\alpha\}$ characterizes the autoionizing bound state manifold of interest, Equation (2) would be applied only to levels $j \in \{\alpha\}$. For practical application, these manifolds may be defined to include states with the same principal quantum numbers, but different angular-momentum combinations, e.g., $\{\alpha\} = \{1s^2 2l^7 3l'^2\}$.

For non-autoionizing single excited states, Griem [1,2] provided a general criterion comparing the relative importance of the spontaneous radiative decay rate A and the electron collisional depopulation rate $n_e \times C$. The LTE is achieved when collisions are much more important than radiative decay, i.e.,

$$n_{e,crit} \times C \gg A \tag{3}$$

Generalizing this expression to arbitrary excited states with a principle quantum number n permits a closed expression for the critical density of H-like ions, where radiative decay is dominated by transitions to the ground state [6]:

$$n_{e,crit} \approx 6 \times 10^{19} \cdot Z^7 \cdot \frac{(n-1)^{2n-2}}{n^3(n+1)^{2n+2}} \cdot \left(\frac{T_e(eV)}{Z^2 Ry}\right)^{1/2} [cm^{-3}] \tag{4}$$

where $n_{e,crit}$ is the critical electron density above which LTE holds for states with a principal quantum number larger than n , $Ry = 13.6 eV$ and Z is the ionic charge. Equation (4) is a

criterion for partial local thermodynamic equilibrium PLTE, i.e., a Boltzmann population for levels with quantum numbers larger than n .

The generalization of Equation (3) for autoionizing states requests the introduction of the autoionization rate Γ (that can even be larger than corresponding radiative decay rates). Figure 1a schematically visualizes the introduction of the autoionization rate on the same footing as Equation (3): Collisional depopulation rates have to exceed the decay given by radiative (A) and non-radiative transitions (Γ). Instead of Equation (3), we obtain:

$$n_{e,crit} \times C \gg A + \Gamma \tag{5}$$

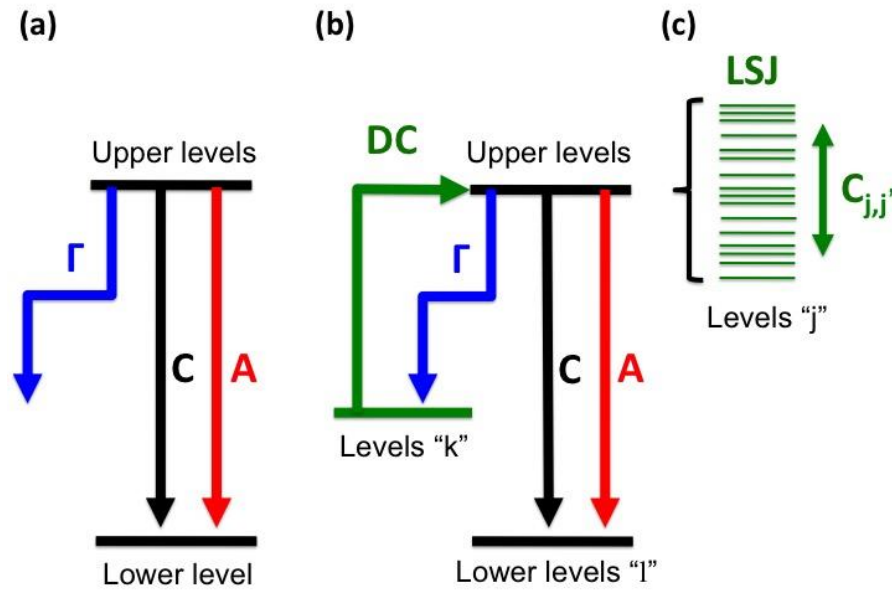


Figure 1. Schematic energy-level diagrams of autoionizing states to study pathways to local thermodynamic equilibrium (Γ is the autoionization rate, C is the collisional rate, A is the radiative decay rate, DC is the dielectronic capture rate, LSJ indicates an LSJ-split-level structure, and $C_{j,j'}$ is the corresponding collisional rates between the LSJ-split levels): (a) standard approach according to Equations (3) and (5), (b) multi-channel diagram, and (c) detailed LSJ-split-level structure of autoionizing states with collisional redistribution.

We note that Equation (5) does not readily lead to a modification of Equation (4), because, for autoionization rates, there are no simple scaling laws available.

Let us therefore illustrate Equation (5) with a numerical example of the autoionizing manifold $\{\alpha\} = \{1s^22l^73l'^2\}$ of aluminum. Figure 2 shows the corresponding level structure and relevant transitions. Figure 3 shows the spectral distribution of the dielectronic satellite transitions that involve three different types of transition:

$$1s^22s^12p^63l^2 \rightarrow 1s^22s^22p^63l^1 + \hbar\omega_{satellite} \tag{6a}$$

$$1s^22s^22p^53l^2 \rightarrow 1s^22s^22p^63l^1 + \hbar\omega_{satellite} \tag{6b}$$

$$1s^22s^12p^63l^2 \rightarrow 1s^22s^22p^53l^2 + \hbar\omega_{satellite} \tag{6c}$$

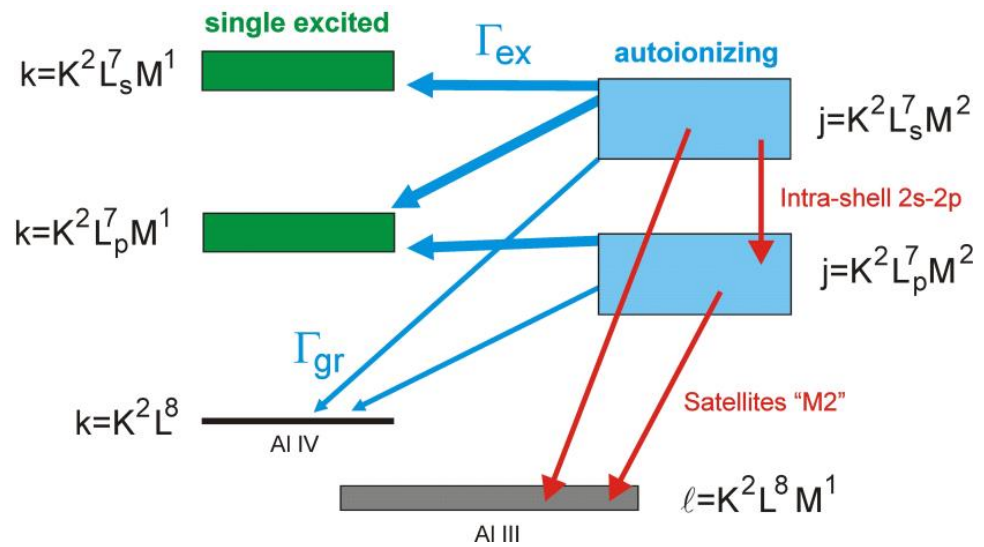


Figure 2. Energy-level diagram of the autoionizing manifold $\{1s^2 2l^7 3l'^2\}$ with relevant transition rates. The short hand notation $L_p^7 = 2s^2 2p^5$ and $L_s^7 = 2s^1 2p^6$ is introduced. Blue flashes indicate autoionizing rates, red ones spontaneous transitions.

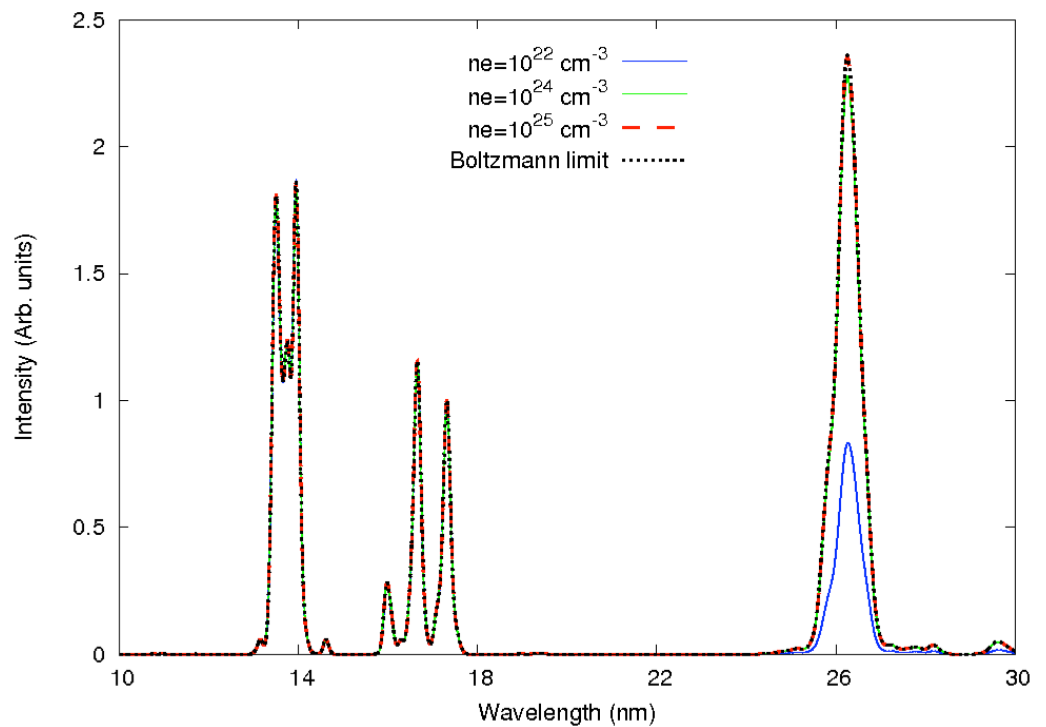


Figure 3. Spectral distribution originating from the autoionizing manifold $\{1s^2 2l^7 3l'^2\}$ of Mg for different electron densities and electron temperature $k_B T_e = 25 \text{ eV}$. Gaussian line profiles are assumed to better visualize population effects on the spectral distribution. Strong deviations are seen near 26 nm (blue curve).

As demonstrated by Figure 3, transitions (6a) are essentially located around 14 nm, transitions (6b) are around 17 nm, and intra-shell transitions are near 26 nm. Spectral distributions are calculated according Equation (1), while population densities are calculated from collisional-radiative population kinetics (taking into account all LSJ-split autoionizing and non-autoionizing levels of Al III). Figure 3 also shows that the spectral distribution ap-

proaches the LTE distribution (indicated in the figure as the “Boltzmann limit”) at electron densities of about 10^{24} – 10^{25} cm^{-3} .

Employing the FAC atomic structure code [13], we obtain the following averaged quantities relevant for Equation (5): $\bar{C} \sim 10^{-9}$ cm^3s^{-1} , $\bar{A} \sim 10^9$ s^{-1} , and $\bar{\Gamma} \sim 10^{14}$ s^{-1} , from which it follows $n_{e,crit} \gg 10^{23}$ cm^{-3} . This estimate seems to be in agreement with the simulations presented in Figure 3 for the various electron densities: the spectral distribution calculated for $n_e = 10^{24}$ cm^{-3} is rather close to the Boltzmann limit, while the distribution calculated for $n_e = 10^{22}$ cm^{-3} is quite far from the LTE case (see in particular the large deviations around 26 nm).

The critical electron density according Equation (5) is therefore much larger than solid density, and the LTE assumption would not be satisfied for the overwhelming number of experimental cases. This conclusion would be a general one, because autoionization rates are typically of the order of $\bar{\Gamma} \sim 10^{13} - 10^{15}$ s^{-1} and do not strongly depend on charge Z . In fact, in the simple H-like model, the autoionization rate is even independent of Z , i.e., $\bar{\Gamma} \propto Z^0$. Therefore, large critical densities are also related to low-charged ions, while in the standard case of single excited states (Equation (3)), the strong scaling of the radiative decay rate with charge, i.e., $\bar{A} \propto Z^4$, implies that critical densities considerably decrease for a low ion charge (Equation (4)).

3. Thermalization of Autoionizing States

The underlying assumptions of Equations (3) and (5) are readily identified comparing the schematic diagrams of Figure 1a,b. The bunch of autoionizing levels “j” is indicated by a single black horizontal line “Upper levels” in Figure 1a,b. Figure 1c visualizes the detailed LSJ-split-level structure for all autoionizing levels “j” and the collisional redistribution (indicated by the collisional rate coefficients $C_{j,j'}$) between these levels. Figure 1a shows a single-channel approach: only depopulation rates are considered while the collisional rates are compared with all other processes to obtain relations (3) and (5). Figure 1b is conceptually different. The multi-channel approach considers depopulation and population. This allows for the possibility that the population flow (indicated by “DC” in Figure 1b) contributes to thermalization, thereby reducing the “work load” of collisions (indicated with “C” in Figure 1b,c), which implies a reduction in the critical density. Likewise, it may allow for the possibility that this population flow works against thermalization, implying an increase in the critical density.

Below it will be demonstrated that the inclusion of the multi-channel “DC” can result only in a reduction in the critical density.

3.1. Multi-Channel Approach

In order to study the impact of multi-channels on critical densities in analytical form, we consider quasi-stationary population kinetics related to the autoionizing manifold $\{\alpha\}$ for one level “l” and one level “k” (see Figure 2):

$$n_j \cdot (\Gamma_{j,k} + A_{jl} + n_e \cdot C_{jl} + n_e \cdot C_{jj'}) \approx n_e n_k \cdot DC_{k,j} + n_e n_l \cdot C_{lj} \quad (7)$$

For our cases of interest, the autoionization rate $\Gamma_{j,k}$ is much higher than the radiative A_{jl} and collisional $n_e C_{jl} + n_e C_{jj'}$ ones, and dielectronic capture dominates over inner-shell excitation. Equation (7) then simplifies to:

$$n_j \cdot \Gamma_{j,k} \approx n_e n_k \cdot DC_{k,j} \quad (8)$$

The dielectronic capture (inverse process of autoionization) rate coefficient $DC_{k,j}$ is given by:

$$DC_{k,j} = \frac{1}{2} \cdot \left(\frac{2\pi\hbar^2}{m_e} \right)^{3/2} \cdot \frac{g_j}{g_k} \cdot \Gamma_{j,k} \cdot \frac{\exp\left(-\frac{E_j - E_k}{k_B T_e}\right)}{(k_B T_e)^{3/2}} \quad (9)$$

where $E_{j,k} = E_j - E_k$ is the (positive) capture energy (capture from state “ k ” to the autoionizing level “ j ”), m_e is the electron mass, and g_j and g_k are the statistical weights. Let us now consider a couple of levels (k, j) and (k', j') and form the ratio of Equations (8) and (9):

$$\frac{n_j}{n_{j'}} \approx \frac{n_k}{n_{k'}} \cdot \frac{g_{k'}}{g_k} \cdot \frac{g_j}{g_{j'}} \cdot \frac{\exp\left(-\frac{E_j - E_k}{k_B T_e}\right)}{\exp\left(-\frac{E_{j'} - E_{k'}}{k_B T_e}\right)} \quad (10)$$

The levels “ k ” are single excited levels where the standard thermalization criteria (2) with corresponding relatively low critical densities apply. E.g., for the present example of the manifold $\{\alpha\} = \{1s^2 2l^7 3l'^2\}$, the critical densities for the levels “ k ” (see also Figure 2) are several orders of magnitude lower than those provided by Equation (5) for the autoionizing levels “ j ”. Let us therefore assume that levels “ k ” are populated essentially according Boltzmann, i.e.,

$$\frac{n_k}{n_{k'}} \approx \frac{g_k}{g_{k'}} \cdot \exp\left(-\frac{E_k - E_{k'}}{k_B T_e}\right) \quad (11)$$

Inserting (11) into (10) results in:

$$\frac{n_j}{n_{j'}} \approx \exp\left(-\frac{E_k - E_{k'}}{k_B T_e}\right) \cdot \frac{g_j}{g_{j'}} \cdot \frac{\exp\left(-\frac{E_j - E_k}{k_B T_e}\right)}{\exp\left(-\frac{E_{j'} - E_{k'}}{k_B T_e}\right)} \quad (12)$$

from which it follows:

$$\frac{n_j}{n_{j'}} \approx \frac{g_j}{g_{j'}} \cdot \exp\left(-\frac{E_j - E_{j'}}{k_B T_e}\right) \quad (13)$$

Equation (13) means that thermalization between the autoionizing levels has occurred. The important difference of Equation (13) as derived from Equations (7)–(12) rather than derived directly from Criteria (5) is that only critical densities that are related to the “ k -levels” are involved rather than to the autoionizing levels “ j ” themselves. This results in critical densities that are smaller by orders of magnitude, as visualized in Figure 4.

According to Equations (7)–(13), the thermalization of the autoionizing levels is achieved without involving collisions between the autoionizing levels themselves. This is conceptually different from the standard criteria (2) or (5). The key question is now: Does Equation (8) relate to cases of practical interest? It will be shown below that this is really the case and in particular holds true if capture to excited states exists.

3.2. Boltzmann-like Population Flow Driven by Inverse Autoionization

Physically, the multi-channel approach (Figure 1b) acts with the population flow “DC” (see Figure 1b) into autoionizing levels like a “Boltzmann flow” into the autoionizing manifold, while the Boltzmann-like feature is established by collisions between the capture states “ k ” rather than by collisions between the autoionizing states “ j ”.

The necessary conditions to apply Equation (13) are related to the transition from Equation (7) into Equation (8), i.e., that almost all autoionizing rates are dominating for the autoionizing manifold. In order to study this condition in detail, we performed Multi-Configuration-Dirac-Fock atomic structure calculations, including intermediate coupling and configuration interaction with the FAC code to obtain the autoionization and radiative decay rates for all LSJ-split levels.

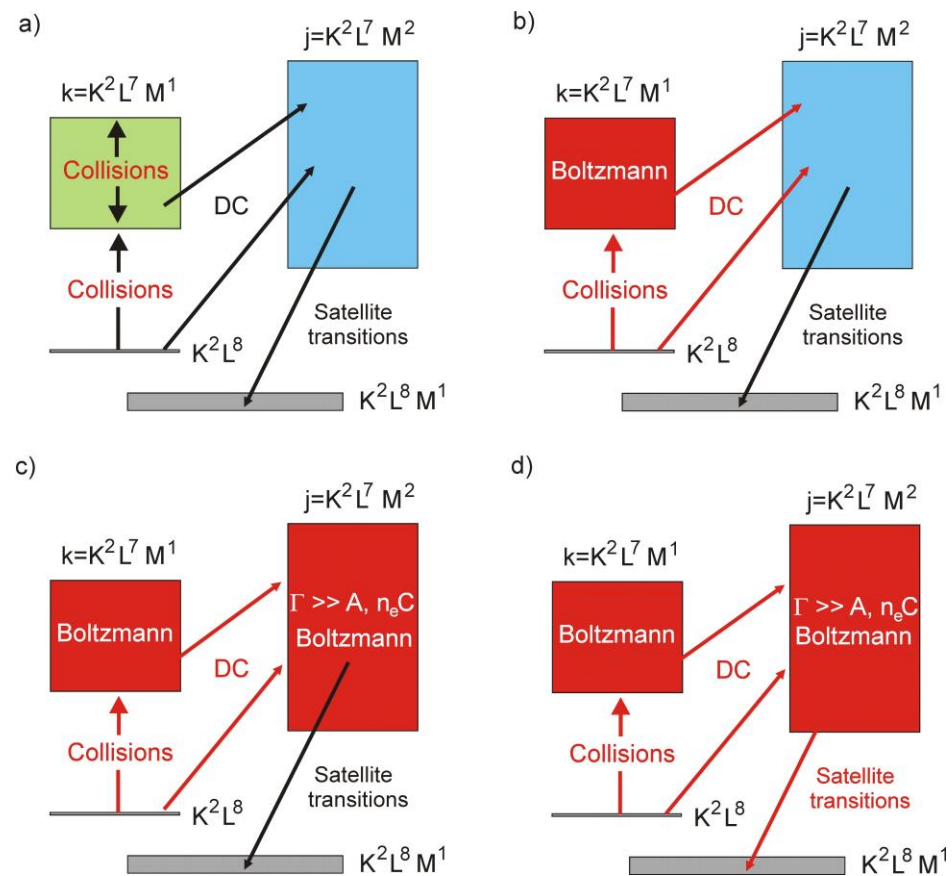


Figure 4. Schematic illustration of the steps to achieve a Boltzmann distribution between autoionizing levels without invoking collisions between the autoionizing levels itself. (a) Collisions drive non-thermal excited-state populations of the levels $k = K^2 L^7 M^1$, from which effective dielectronic capture to the autoionizing levels $j = K^2 L^7 M^2$ occurs, followed by spontaneous radiative satellite emission. (b) High collisions drive single excited-state levels k into a Boltzmann population, followed by a statistical population flow of dielectronic capture to autoionizing levels j . If Equation (8) holds true (visualized by $\Gamma \gg A, n_e C$), the autoionizing levels j are likewise populated according Boltzmann, (c) the statistical population flow results into a Boltzmann population of the autoionizing levels if the autoionization rates (Γ) are much larger than collisional ($n_e C$) and radiative decay rates (A). Finally, a Boltzmann spectral distribution (d) originates from the autoionizing levels j .

Interference effects between autoionization and radiative decay [14] are not included. These effects are of particular importance for energy resolved studies on autoionization. This is not the case in plasmas, where the frequent collisions between continuum electrons result in a very broad energy distribution function. Consequently, only the integral over the resonance function is of importance. E.g., if radiative decay rates are about a factor of two larger than autoionization rates (a typical case for highly charged iron), the interference calculations differ only slightly from standard ones [15]. In the case where radiative decay is dominating (typically the case for highly charged Xenon), the resonance case may differ considerably between the two types of calculations, but, as in the case of iron, the total integrals differ again much less dramatically.

Moreover, as interference effects are of importance for the total rates of autoionization and radiative decay if the radiation decay rate is much larger than the autoionization rate, a relevant “interference case” does not really correspond to the present multi-channel approach that requests autoionization rates much larger than radiative decay rates.

Figure 5 shows the distribution of the autoionization and radiative decay rates for all levels of the autoionizing manifold (indicated by level numbers 42–278), while Table 1 summarizes the averaged data. Three important observations can be drawn from Figure 5

and Table 1: first, autoionizing rates are, by many orders of magnitude, larger than radiative decay rates, second, large autoionization rates are distributed rather smoothly over all autoionizing levels $1s^2 2s^2 2p^6 3l 3l'$, and third, autoionization to excited states is 1–2 orders more important than to the ground state. These properties assure a rather homogenous Boltzmann-like flow all over all autoionizing levels “j” driven from the levels “k”.

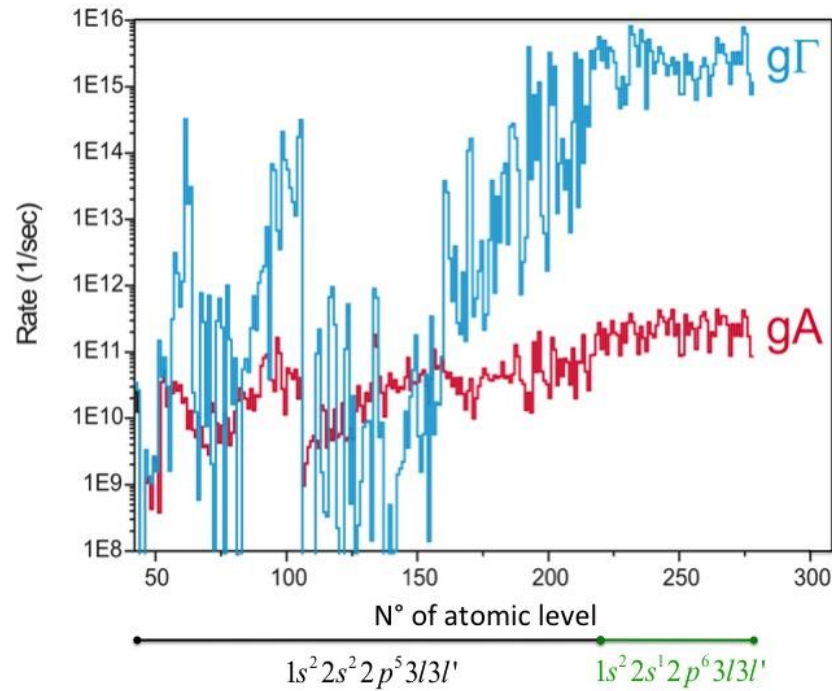


Figure 5. Distribution of the radiative decay and autoionizing rates over the various levels of Mg that are designated by numbers. The number “0” corresponds to the Ne-like ground state, the numbers “1. . .36” are the single excited levels $1s^2 2l^8 3l'^1$ (depicted as levels “k” in Figure 2) and the numbers “37. . .41” are the Na-like levels $1s^2 2l^8 3l'$ (depicted as levels “l” in Figure 2). The numbers “42. . .278” are the autoionizing levels $1s^2 2l^7 3l'^2$ (depicted as levels “j” in Figure 2) that are distinguished by different core hole configurations ($1s^2 2s^2 2p^5 3l'^2$ black line with black designation, $1s^2 2s^1 2p^5 3l'^2$ green line with green designation).

Table 1. Averaged autoionization and radiative decay rates of aluminum for the manifold $\{1s^2 2l^7 3l'^2\}$ calculated with the Multi-Configuration-Dirac-Fock method. including intermediate coupling and configuration interaction.

Autoionization rates [s^{-1}]		
	$1s^2 2s^2 2p^5 3l 3l'$	$1s^2 2s^1 2p^6 3l 3l'$
$1s^2 2s^2 2p^6$	2.2×10^{12}	1.1×10^{12}
$1s^2 2s^2 2p^5 3l$	2.1×10^{13}	5.4×10^{14}
$1s^2 2s^1 2p^6 3l$	-	2.1×10^{13}
Radiative decay rates [s^{-1}]		
$1s^2 2s^2 2p^6 3l$	3.8×10^9	2.4×10^9
$1s^2 2s^2 2p^5 3l 3l'$	-	4.1×10^{10}

From the atomic structure point of view, the rather homogenous distribution of radiative decay and autoionization rates is a consequence of the multi-electron open shell configurations, where configuration interaction and electron–electron interaction are impor-

tant. Therefore, the “atomic structure complexity” of the autoionizing manifold facilitates thermalization.

3.3. Numerical Calculations

In order to validate the analytical estimates, we present below detailed numerical calculations. For this purpose, we established a multi-level multi-ion charge state system of atomic population kinetic equations to calculate the level populations $n_i^{(Z)}$ for the ground, single, and multiple-excited states for various charge states. The collisional-radiative processes include all radiative electric dipole transitions, autoionization to ground and single-excited states, dielectronic capture from ground and single-excited states, collisional excitation and de-excitation, ionization, three-body recombination, and radiative recombination in an LSJ-split level structure. Atomic structure, levels, and rate coefficients were obtained from the FAC code, taking into account configuration interaction and intermediate coupling. The selected plasma parameters are relevant to an XUV-FEL experiment, where the focused beam was brought to interact with solid aluminum [16].

Figure 6 shows the spectral distribution of the relevant satellite emissions for $k_B T_e = 25$ eV and various electron densities; the Boltzmann limit is indicated by the dashed black curve. It is observed that for electron densities $n_e = 10^{20}$ cm⁻³, the spectral distribution is close to LTE and, at $n_e = 10^{21}$ cm⁻³, the distribution is almost identical to the LTE case. This indicates that the Boltzmann flow from the single-excited states $k \in \{1s^2 2l^7 3l'\}$ is so effective that the critical electron density $n_{e,crit}$ above which the LTE holds is decreased by almost four orders of magnitude (compared to Figure 3 that does not include the capture channel from the levels k).

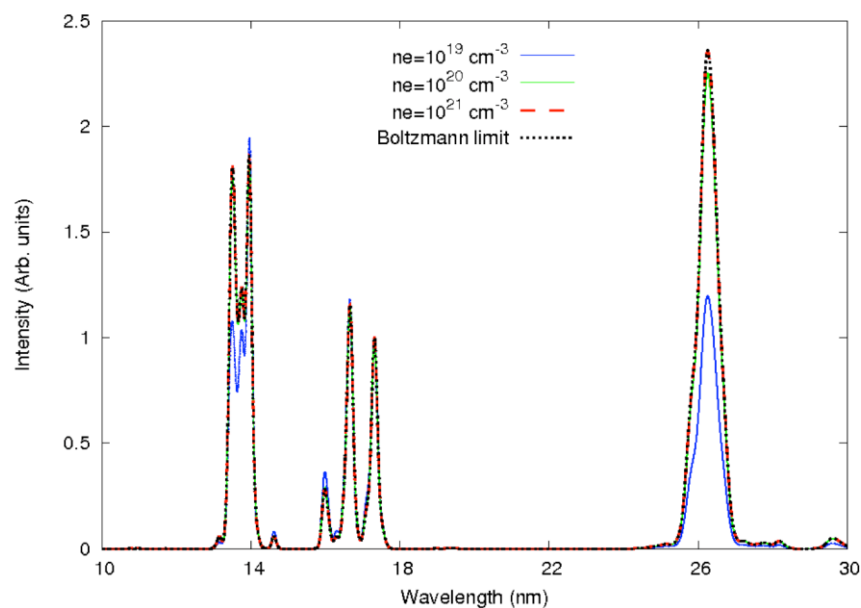


Figure 6. Spectral distribution of Mg for different electron densities and electron temperature of $k_B T_e = 25$ eV obtained from a population kinetic collisional-radiative approach involving LSJ-split level structure and multi-charge states. Strong deviations are seen near 14 nm and 26 nm (see blue curve).

The contribution of the Boltzmann flow from the levels “ k ” to the autoionizing manifold depends on the absolute population of these levels, being strongly dependent on the ionic charge state distribution. The charge state distribution does not only depend on temperature and density, but on the transient evolution too.

3.4. Transient Plasma Evolution

Let us characterize the transient plasma evolution by the ground state population ratio of Al IV and Al III via the parameter $r = n_{gr}^{Al IV} / n_{gr}^{Al III}$. Figure 7 shows simulations that cover two orders of magnitude different r-values and one order of magnitude in temperature (and is therefore relevant to almost all experimental conditions). It can directly be seen that, for all cases, the exact simulations carried out for $n_e = 10^{22} \text{ cm}^{-3}$ are almost identical to the LTE case. This means that, for almost all cases of practical interest, the critical electron density above which LTE holds is lower by two...three orders of magnitude compared to the case depicted in Figure 3.

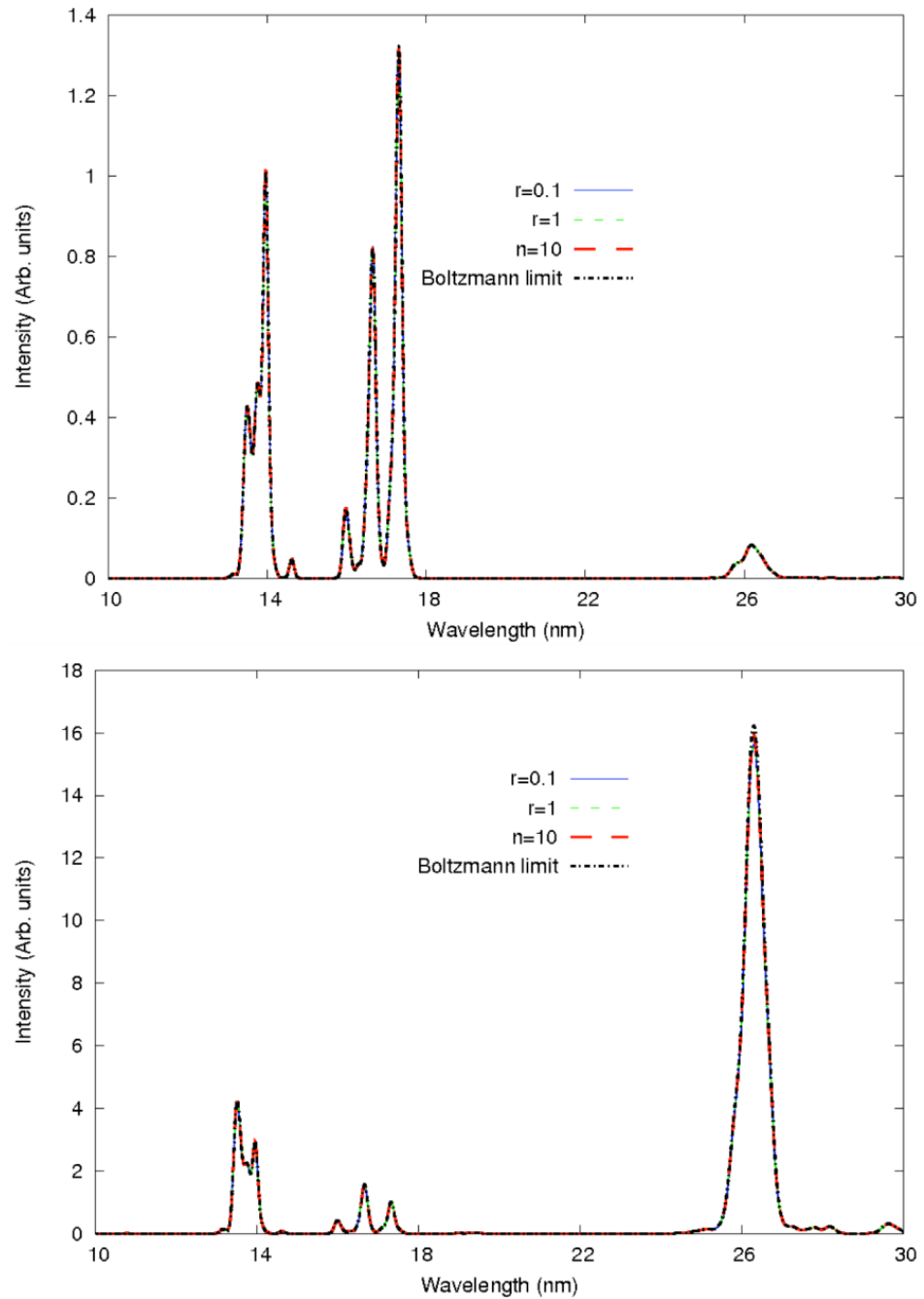


Figure 7. Spectral distribution of the dielectronic satellite emission of Mg calculated for $n_e = 10^{22} \text{ cm}^{-3}$, $k_B T_e = 10 \text{ eV}$ (upper figure) and $k_B T_e = 100 \text{ eV}$ (lower figure) for different ratios r of the ground state populations of Al^{3+} and Al^{2+} .

In view of this analysis, the criterion (5) is identified as a theoretical limiting case, where the charge state that corresponds to levels “k” has vanishing population: if the charge state of the autoionizing manifold is Z with a population n_j^Z , then the charge state of levels “k” is $Z - 1$ and a vanishing population then means $n_k^{Z-1} = 0$.

4. Summary of Criteria for Critical Densities

Let us now compare the various criteria and related critical electron densities.

4.1. Single Excited and Non-Autoionizing States

In this case, the well-known criterion of Griem applies, i.e.,

$$n_{e,crit} \times C_{depop} \gg A_{depop} \tag{14}$$

where $n_{e,crit}$ is the critical electron density above which the thermalization of atomic states can be assumed, C_{depop} is the electron–ion collisional depopulation rate coefficient, and A_{depop} is the spontaneous radiative decay rate that depopulates the upper level. Usually, one is interested in the thermalization of a certain bunch of upper levels, i.e., a manifold (e.g., $\{\alpha\} = \{1s5l\}$), and C_{depop} would essentially correspond to $C_{depop}(1s5l \rightarrow 1s5l')$, because collisions in the fine structure $1s5l$ are dominating, and A_{depop} is dominated by $A_{depop}(1s5l \rightarrow 1s^2)$ because radiative decay to the ground state is dominating.

4.2. Autoionizing Levels: Single-Channel Approach

Like in Griem’s criterion, the single-channel approach (Figure 1b) only takes into account depopulating processes, we therefore have:

$$n_{e,crit} \times C_{depop} \gg A_{depop} + \Gamma_{depop} \tag{15}$$

where Γ_{depop} is the depopulation rate of the upper level via non-radiative decay (autoionization), including decay to ground and excited states. We note that, for autoionization, decay to excited states is usually much larger than decay to the ground state, see Table 1. This implies that criterion (5) results in much higher critical densities (orders of magnitude) than criterion (14).

4.3. Autoionizing Levels: Multi-Channel Approach

Although the estimate according Equation (15) is not wrong, it is of little practical interest, because it usually delivers critical electron densities much above solid density. The practical interest is in a criterion that provides much less stringent conditions to assure the thermalization of all levels “j” of an autoionizing manifold $\{\alpha\}$. This can be formulated as follows if autoionization (with corresponding autoionization rates $\Gamma_{j,k}$) proceeds toward a manifold $\{k\}$:

$$n_{e,crit} \times C_{depop}(k) \gg A_{depop}(k) \tag{16a}$$

$n_{e,crit}$ is the critical electron density above which the thermalization of the atomic states $\{k\}$ can be assumed, $C_{depop}(k)$ is the electron–ion collisional depopulation rate coefficient and $A_{depop}(k)$ is the spontaneous radiative decay rate that depopulates the levels $\{k\}$.

Condition (16a) has to be supplemented with the request that, within the autoionizing manifold $\{\alpha\}$, autoionizing rates exceed globally radiative decay rates and collisional rates, i.e., according Equations (7) and (8):

$$\Gamma_{j,k} \gg A_{j,l}, n_e C_{jl} + n_e C_{jj} \tag{16b}$$

$$n_e n_k \cdot DC_{k,j} \gg n_e n_l \cdot C_{lj} \tag{16c}$$

Condition (16b) is a complementary relation to (15) and of particular practical interest, as it does not directly enter into Equation (16a), while it does for relation (5). Relation

(16c) means that dielectronic capture should dominate over inner-shell excitation (see Equations (7) and (8)).

5. Conclusions

We considered pathways to Local Thermodynamic Equilibrium (LTE) in atomic physics for autoionizing states. The standard criterion where collisional rates have to exceed considerably radiative ones in order to determine the critical densities $n_{e,crit}$ (above which atomic levels are populated according Boltzmann) was extended to autoionizing states. It was demonstrated that the extended criterion $n_{e,crit} \times C \gg A + \Gamma$ provided densities exceed considerably exceeded solid densities for many cases of practical interest $\Gamma \gg A$. This held true in particular for complex autoionizing manifolds that decayed not only to the ground state, but to excited states too $\Gamma_{j,k>1}(j \rightarrow \text{excited states})$. Also, for low-charged ions, huge critical densities were predicted, as dominating autoionizing rates were rather independent of the ion charge.

We introduced a new criterion, where the critical density was given by the criterion $n_{e,crit} \times C(k) \gg A(k)$ related to the capture states “k” rather than to the autoionizing levels “j” themselves (supplemented by the conditions $\Gamma_{j,k} \gg A_j$ and that dielectronic capture dominated over inner-shell excitation). Detailed considerations were carried out for the autoionizing manifold $K^2L^7M^2$ of low-charged Al III. While the standard criterion $n_{e,crit} \times C(j) \gg A(j) + \Gamma_{j,k}$ provides critical densities of about 10^{24} cm^{-3} , the new criterion provides only 10^{21} cm^{-3} , being in excellent agreement with the numerical calculations.

Author Contributions: The authors contributed equally to this work. All authors have read and agreed to the published version of the manuscript.

Funding: This research received no external funding.

Data Availability Statement: The data that support the findings of this study are available from the corresponding author upon reasonable request.

Acknowledgments: Support from the project ‘Emergence 2010: Métaux transparents créés sous irradiations intenses émises par un laser XUV/X à électrons libres’ of the University Pierre and Marie Curie and the Extreme Matter Institute EMMI are greatly appreciated.

Conflicts of Interest: The authors declare no conflict of interest.

References

1. Griem, H. *Plasma Spectroscopy*; McGraw-Hill: New York, NY, USA, 1964.
2. Griem, H. *Principles of Plasma Spectroscopy*; Cambridge University Press: Cambridge, UK, 1997; ISBN 0-521-45504-9.
3. Fujimoto, T. *Plasma Spectroscopy*; Clarendon Press: Oxford, UK, 2004.
4. Lisitsa, V.S. *Atoms in Plasmas*; Springer: Berlin/Heidelberg, Germany, 1994.
5. Salzman, D. *Atomic Physics in Hot Plasmas*; Oxford University Press: Oxford, UK, 2000.
6. Rosmej, F.B.; Astapenko, V.S.; Lisitsa, V.S. *Plasma Atomic Physics*; Springer Series on Atomic, Optical, and Plasma Physics; Springer: Cham, Switzerland, 2021; Volume 104, ISBN 978-3-030-05966-8.
7. Fujimoto, T.; McWhirther, R.W.P. Validity criteria for local thermodynamic equilibrium in plasma spectroscopy. *Phys. Rev. A* **1990**, *42*, 6588. [[CrossRef](#)]
8. Moore, R.M. Pressure Ionization, Resonances, and the Continuity of Bound and Free States. *Adv. Ad. Mol. Phys.* **1985**, *21*, 305.
9. Li, X.; Rosmej, F.B. Analytical approach to level delocalization and line shifts in finite temperature dense plasmas. *Phys. Lett. A* **2020**, *384*, 126478. [[CrossRef](#)]
10. Jha, A.K.S.; Dimri, M.; Dawra, D.; Mohan, M. Study of Atomic Processes for Highly Charged Ions Embedded in Dense Plasma, Special Issue “Atomic Physics in Dense Plasmas”, S.I. Editor: F.B. Rosmej. Available online: https://www.mdpi.com/journal/atoms/special_issues/47A3007EF7 (accessed on 5 November 2023).
11. Janev, R.K.; Zhang, S.; Wang, J. Review of quantum collision dynamics in Debye plasmas. *Matter Radiat. Extremes* **2016**, *1*, 237. [[CrossRef](#)]
12. Rosmej, F.B. An alternative method to determine atomic radiative emission. *Europhys. Lett.* **2006**, *76*, 1081. [[CrossRef](#)]
13. Gu, M.F. The flexible atomic code. *Can. J. Phys.* **2008**, *86*, 675. [[CrossRef](#)]
14. Armstrong, L.; Theodosiou, C.E.; Wall, M.J. Interference between radiation emission and autoionization in the decay of excited states of atoms. *Phys. Rev. A* **1978**, *18*, 2538. [[CrossRef](#)]

15. Sakimoto, K.; Terao, M.; Berrington, K.A. Effects of radiative decay on the bound-continuum transition of highly charged atomic ions. *Phys. Rev. A* **1990**, *42*, 291. [[CrossRef](#)] [[PubMed](#)]
16. Galtier, E.; Rosmej, F.B.; Riley, D.; Khattak, F.Y.; Heimann, P.; Lee, R.W.; Nelson, A.J.; Vinko, S.M.; Whitcher, T.; Wark, J.S.; et al. Decay of crystalline order and equilibration during solid-to-plasma transition induced by 20-fs microfocused 92 eV Free Electron Laser Pulses. *Phys. Rev. Lett.* **2011**, *106*, 164801. [[CrossRef](#)] [[PubMed](#)]

Disclaimer/Publisher's Note: The statements, opinions and data contained in all publications are solely those of the individual author(s) and contributor(s) and not of MDPI and/or the editor(s). MDPI and/or the editor(s) disclaim responsibility for any injury to people or property resulting from any ideas, methods, instructions or products referred to in the content.